Available online at www.sciencedirect.com
ScienceDirect
Journal of the European Ceramic Society 30 (2010) 875–887
www.elsevier.com/locate/jeurceramsoc

Influence of panel/back thickness on impact damage behavior of alumina/aluminum armors

Zhang Zuoguang [a,*], Wang Mingchao [a], Song Shuncheng [b], Li Min [a], Sun Zhijie [a]

[a] School of Materials Science and Engineering, Key Laboratory of Aerospace Materials and Performance (Ministry of Education), Beihang University, Beijing 100191, China
[b] School of Mechanics and Engineering, Southwest Jiaotong University, Chengdu 610031, China

Received 7 December 2008; received in revised form 20 August 2009; accepted 27 August 2009
Available online 6 November 2009

Abstract

Using modified SHPB device, damage behaviors of alumina/aluminum armors under impact load were studied. The influences of panel/back thickness on the target damage characteristics were investigated. The transmitted stress wave increased and the reflected stress wave decreased distinctly with the increase of back thickness, while the panel thickness variation had little influence on the stress wave propagation features. The vertex angle of ceramic inverted cone increased with the increase of back thickness and decrease of panel thickness, but the number of radial cracks reduced with the increase of back thickness and the decrease of panel thickness. Furthermore, the failure mechanism of the ceramic panels, including the cone and radial cracks formation mechanism was analyzed. A "composite beam" model has been established to estimate the local bending stress. The model calculation showed that the local bending stress is related to the panel thickness, back thickness and the panel/back moduli ratio.

Keywords: Armor; Impact; Split Hopkinson pressure bar; Stress wave; Damage mechanism

1. Introduction

Ceramic composite armors have lower density and higher level of protection ability compared to traditional metal armors. They can enhance the viability and battle efficiency of the weapon systems by reducing weight and increasing mobility. Therefore, the ceramic composite armors have been widely used in aircrafts, ground vehicles, ships, individual protections and some other fields in last several decades. Since the damage mechanism of ceramic armors under impact loads is a key for armor structure design and ballistic performance evaluation, great efforts have been put into the impact damage mechanism study for ceramic armors.[1–7]

The velocity of bullet hitting on armor is usually of 500–1500 m/s, which falls into the range of high-speed dynamic impact, so the quasi-static mechanical properties of materials can not be used directly in armor design. In practice, the ballistic impacts have to be carried out for armor structure design and ballistic performance evaluation.[8,9] However, ceramic armors are usually destroyed severely by high-velocity-projectile and little usable information can be gathered after attack. For this reason, the damage mechanism study of ceramic armors by using ballistic impact is very difficult.

Hopkinson bar experimental technique has been commonly used in dynamic mechanical property study of engineering materials.[10–13] Hopkinson bar can provide different impact velocities and record the complete stress wave information during impact, so it is very suitable for impact damage mechanism study. In addition, since the velocity of incident bar is usually several to dozens of meters per second, the penetration of incident bar into ceramic armors causes less damage. This will be beneficial for the damage appearance maintenance and failure mechanism analysis.

In the present work, the impact damage behaviors of alumina/aluminum armors were studied by using the split Hopkinson pressure bar (SHPB) device. Especially, the influences of panel/back thickness on the damage characteristics and stress wave propagation of the composite armors were investigated in

* Corresponding author.
E-mail address: zgzhang@buaa.edu.cn (Z. Zuoguang).

0955-2219/$ – see front matter.
doi:10.1016/j.jeurceramsoc.2009.08.023

Table 1
Structure of alumina/aluminum composite armors.

Target	Panel thickness/mm	Back thickness/mm	Target	Panel thickness/mm	Back thickness/mm
A4A3	4	3	A4A6	4	6
A5A3	5	3	A5A6	5	6
A6A3	6	3	A6A6	6	6
A9A3	9	3	A9A6	9	6
A6A4	6	4	A6A9	6	9

detail, and the damage mechanism of the ceramic panel was discussed. The results will be very useful to the ceramic composite armors design.

2. Experimental

2.1. Targets preparation

The square composite armor targets were composed of alumina panel and 2A12 aluminum alloy back. The sides of the target were 50 mm long. Structures of the targets studied are listed in Table 1.

2.2. Modification of SHPB device

In order to simulate the behavior of projectile impacting target better, the incident bar and the transmitted bar of the SHPB device were modified before test. A schematic drawing of the modified SHPB device is shown in Fig. 1. The front end of the incident bar was machined to cone shape. The diameters of the projectile and incident bar are both 14.5 mm. The lengths of the projectile and incident bar are 200 mm and 400 mm, respectively. The end contacting with target of transmitted bar was machined into tubular structure with 36 mm outside diameter and 32 mm inside diameter. The modification of incident bar helps to provide a concentrated load on the composite armor target. The tubular structure design can avoid the infinite support against the target. If using a solid transmitted bar, the target is equivalent to be supported by an infinite back and cannot flex freely. When supported by the tubular transmitted bar, the target can flex locally under impact load, which is more similar to the real behavior of bullet impact on composite armor. A picture of part of the modified SHPB device is shown in Fig. 2.

The modification of incident bar and the transmitted bar changed the one-dimensional stress state in incident bar, sample, and transmitted bar. Therefore, the stress state of tested sample cannot be calculated simply by subtracting the transmitted stress from the incident stress. Although the stress state in the samples cannot be calculated accurately, the difference of stress propagation and absorption between different samples can be obtained by comparing the incident stress and transmitted stress.

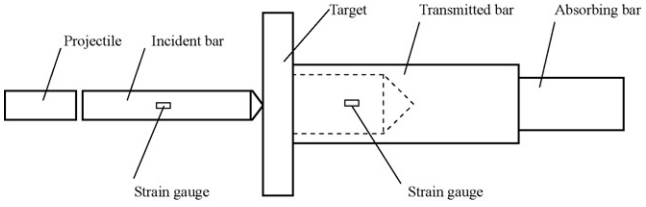

Fig. 1. A schematic drawing of improved SHPB device.

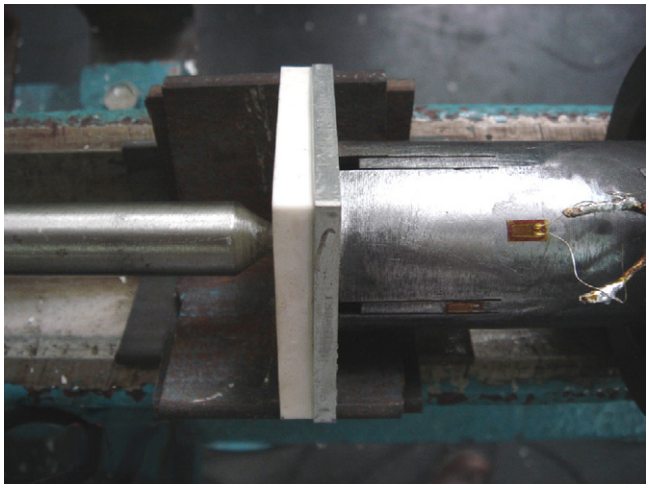

Fig. 2. A photograph of partial improved SPHB device.

2.3. Stress wave characterization

The impact tests were carried out with the projectile velocity of 15 m/s. A series of typical experimental stress waves are shown in Fig. 3. The wave (a) is the incident compression stress wave formed during projectile impact on the incident bar, which wavelength is two times of the projectile length. When

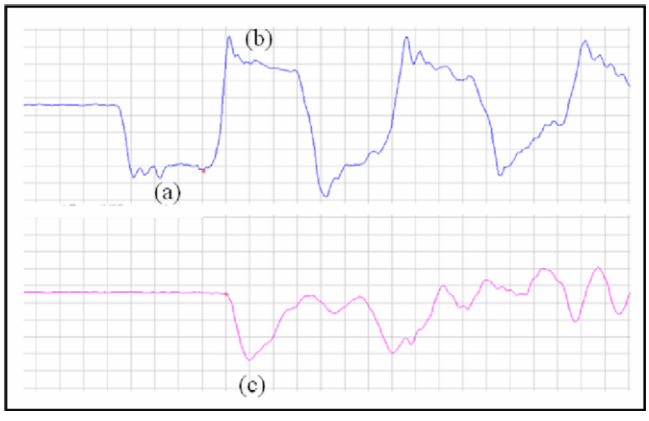

Fig. 3. The stress waves recorded during impact, (a) incident wave; (b) reflected wave; (c) transmitted wave.

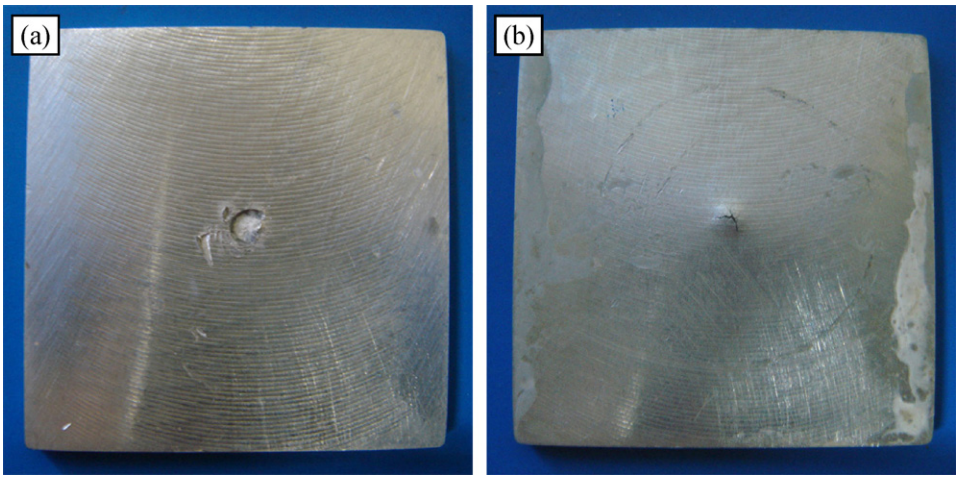

Fig. 4. A typical damage morphology of aluminum back after impact, (a) adhered face; (b) free face.

the incident compression wave reaches the composite armor target, part of it is reflected back forming the reflected tension stress wave (b), while another part passes through the composite armor target and forms the transmitted compression stress wave (c).

The stress wave signals recorded by strain gauges on the incident bar and transmitted bar were voltage signals, by which the strain can be expressed as

$$\varepsilon = 2000 \times 10^{-6} \times V_k \tag{1}$$

where V_k is the voltage signals recorded. Then, the stress can be calculated by the following formula:

$$\sigma = E\,\varepsilon \tag{2}$$

where E is the modulus of the bars.

3. Results and discussion

3.1. Damage morphology analysis of composite armor

In most of the dynamic impact tests, alumina panel cracked into several fragments, debonded and flied away from the aluminum back. The damage of the aluminum back displayed mainly flexural deformation and a penetration crater beneath the impact point, as shown in Fig. 4. Microcracks can be observed on the back of the impact point when the aluminum back is thin. Because the deflection of the aluminum back is difficult to measure and quantify, the armors failure morphology were studied mainly through the investigation of damage appearance of ceramic panels.

Similar to the fracture appearance of bullet impact, the cone crack and radial cracks were observed in the damage of alumina panel under SHPB bar impact.[7] It is believed that the cone crack formation during impact has great contribution to the ballistic resistance enhancement of the ceramic composite armors. The cone vertex angle increase can improve the block and wear abrasion effect of ceramic panel, as well as the response area of back plate.[14] A schematic drawing of the inverted ceramic cone is shown in Fig. 5, from which the relation of several key parameters of the ceramic cone can be constructed as below:

$$\theta = \arctan\left(\frac{d_2 - d_1}{2h_c}\right) \tag{3}$$

where θ is the half cone angle of the inverted ceramic cone; h_c is the thickness of the ceramic panel; d_1 and d_2 are the top and bottom diameters of the ceramic cone, respectively.

Actually, the inverted ceramic cone cracked into small fragments during impact and could not be gathered, and the h_c, d_1 and d_2 were measured from the cone cavity formed in the ceramic panel. Then, the half cone angle θ was calculated by formula (3). Another important damage feature of ceramic panel, the number of radial cracks can be counted directly from the damaged panel.

3.1.1. Influence of the panel thickness

The ceramic damage appearances of the armors with different panel thickness are shown in Fig. 6. The top and bottom circles

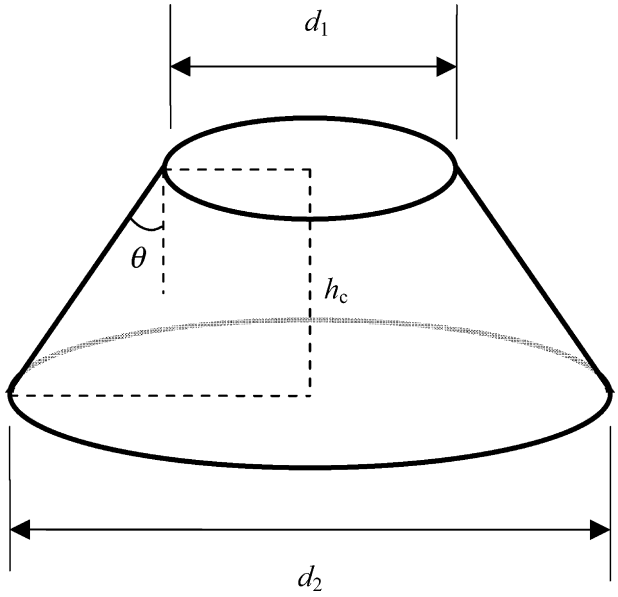

Fig. 5. A schematic drawing of the inverse ceramic cone.

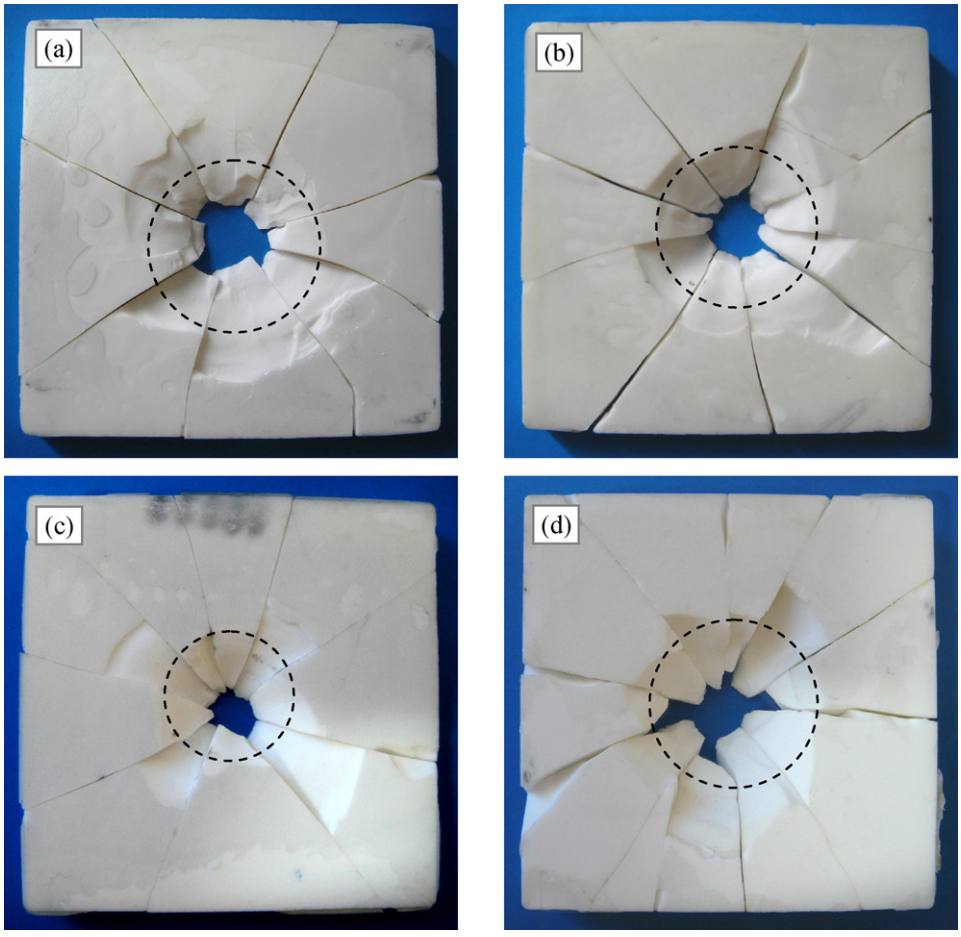

Fig. 6. The ceramic damages of targets with different panel thickness, (a) A4A3; (b) A5A3; (c) A6A3; (d) A9A3.

of ceramic cone cavity of each panel are drawn in Fig. 6, from which the d_1 and d_2 were determined, and then the half cone angle θ were calculated by formula (3). The parameters of cone crack and radial cracks for the targets in Fig. 6 are listed in Table 2. As can been seen from Fig. 6 and Table 2, when the panel thickness increases, the half cone angle θ decreases but the number of the radial cracks increases from 8 to 11. Since the decrease of cone vertex angle and the increase of number of radial cracks are both harmful to the ballistic performance enhancement of the armor,[14] the increase of panel thickness can not improve the ballistic property effectively.

The formation sequence of cone crack and radial cracks can be analyzed briefly from the damage appearances in Fig. 6. The bottom circle of ceramic cone cavity is divided into several sections by the radial cracks. Every two adjacent arc sections are mostly discontinuous in the shown ceramic panels. The discontinuity of the arc sections suggests that the cone crack forms behind the radial cracks. Furthermore, with the increase of panel thickness, the discontinuity of the arc sections becomes more obviously.

3.1.2. *Influence of the back thickness*

The ceramic damage appearances of the armors with different back thickness are shown in Fig. 7, in which the target A6A0 is a 6 mm thick alumina tile without aluminum back. The parameters of cone crack and radial cracks for the targets are listed in Table 3. The number of radial cracks decreases obviously with the increase of back thickness. When the back is thin, there are 8–9 radial cracks in the ceramic panel; when the back thickness increases to 9 mm, there are only 2 radial cracks. At the same time, the cone vertex angle also increases distinctly with the

Table 2
Ceramic damage parameters of targets with different panel thickness.

Target	d_1/mm	d_2/mm	Tangent of θ	θ/°	Number of radial cracks
A4A3	6.7	22.7	2	63.4	8
A5A3	6.1	21.3	1.52	56.6	9
A6A3	5.5	15.5	0.83	39.8	8–9
A9A3	6.1	20.1	0.78	37.8	11

Table 3
Ceramic damage parameters of targets with different back thickness.

Target	d_1/mm	d_2/mm	Tangent of θ	θ/°	Number of radial cracks
A6A0	12	17.8	0.49	35.9	8
A6A3	5.5	15.5	0.83	39.8	8–9
A6A4	5.2	14.1	0.75	36.2	8–9
A6A6	6.2	28.4	1.85	61.6	4–7
A6A9	5.2	31.9	2.22	65.8	2

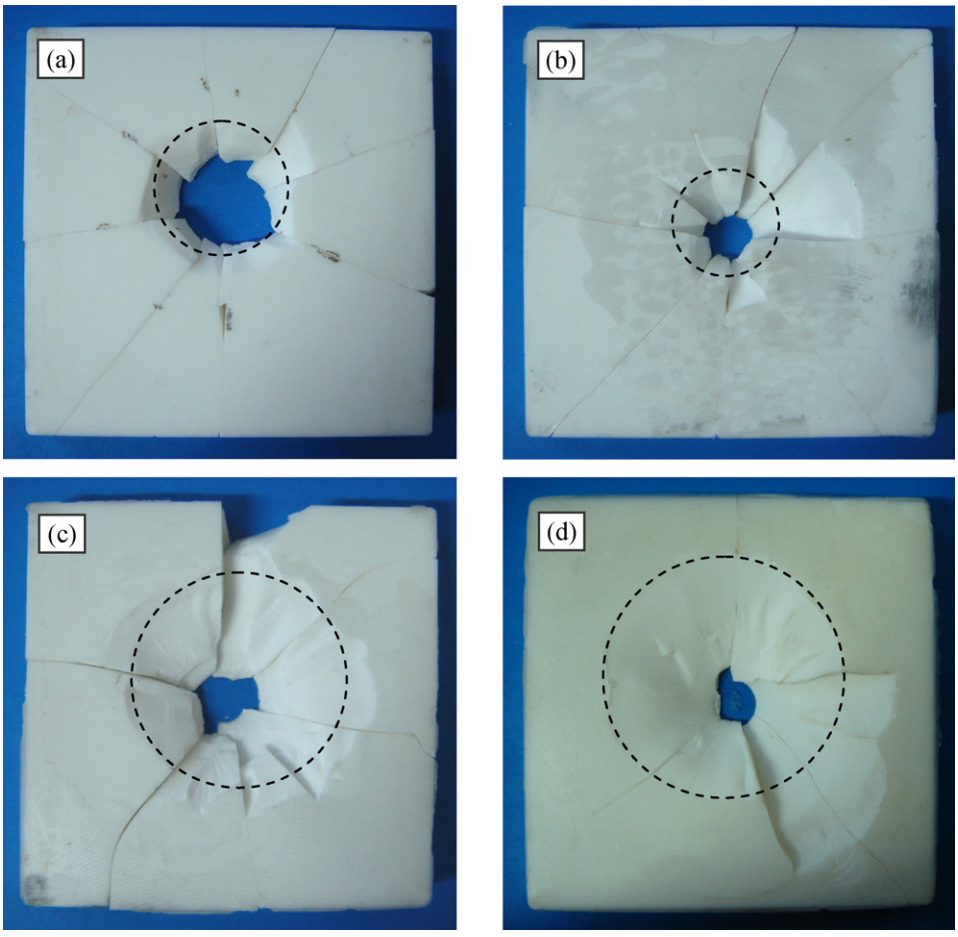

Fig. 7. The ceramic damages of targets with different back thickness, (a) A6A0; (b) A6A4; (c) A6A6; (d) A6A9.

increase of back thickness. For the ceramic composite armor, the increase of cone vertex angle and decrease of the number of radial cracks can improve the bullet resistance of the ceramic inverted cone by enhancing the bullet block and abrasion effect. Compared to last section, it can be found that the influence of back thickness variation on the ballistic performance is quite different from that of panel thickness. The back thickness increase is more positive to the ballistic performance improvement for ceramic composite armors.

The variation of the integrity of the ceramic inverted cone can also be observed from Fig. 7. When the back thickness is less than 4 mm, the bottom circle of cone cavity is divided into interrupted sections by radial cracks. It can be explained as follow. The radial cracks form firstly and cut the ceramic

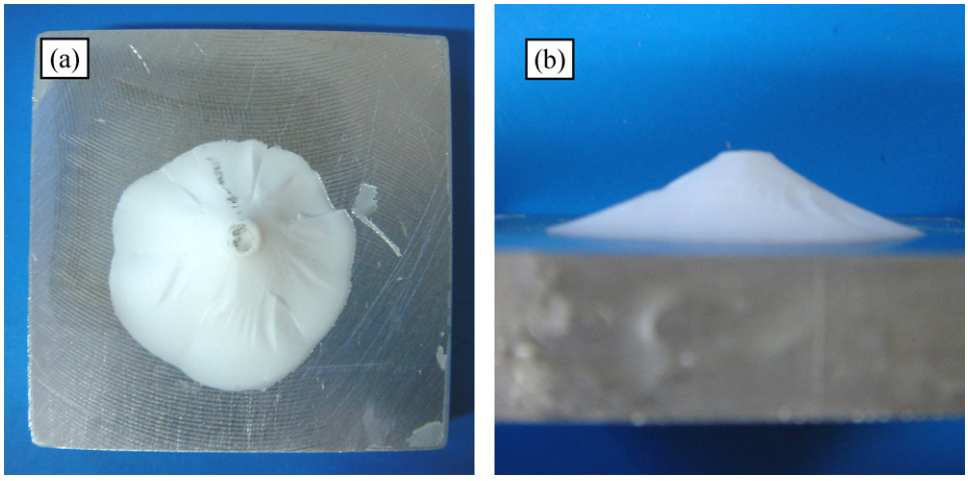

Fig. 8. The integral ceramic inverted cone of target A6A9, (a) vertical view; (b) side view.

panel into several pieces, and then the cone cracks form independently in each piece. As a result, the bottom circle of cone ceramic is naturally discontinuous. When the back is thicker, the cone crack is more integral and smooth as shown in Fig. 7(c) and (d). It suggests that the cone crack formation is earlier than the radial cracks formation. In this case, even though the radial cracks divide the cone crack into several sections, they will not change the continuity of the ceramic cone. Especially in target A6A9, the ceramic inverted cone is complete integral, as shown in Fig. 8. For the integrity of inverted cone is conducive to the block effect of ceramic panel on bullet penetration, the back thickness increase can improve the ballistic performance effectively.

3.2. Stress wave feature analysis of composite armors

3.2.1. Influence of the panel thickness

In order to discuss the influence of panel thickness on the stress wave feature of composite armors better, the stress waves of two series of targets with 3 mm-thick back and 6 mm-thick back are investigated in Figs. 9 and 10, respectively. The characteristic values of stress waves of the targets in Figs. 9 and 10 are listed in Table 4. The wave lengths in Table 4 are expressed with propagating time and the intensity are expressed with the voltage recorded by strain gauges. To eliminate the influence of the variation of incident wave intensity, the specific intensities of reflected wave and transmitted wave were introduced. They were defined as ratios of the absolute values of intensities of reflected wave and transmitted wave to the intensity of incident wave, respectively.

When the back thickness is the same, the change of the reflected waves and transmitted waves of different targets is indistinct in Figs. 9 and 10. Referring to the data in Table 4, the specific intensity of transmitted wave improves with the increase of panel thickness. For example, when the back thickness is 3 mm and the panel thickness increases from 3 mm to 9 mm, the specific intensity of transmitted wave increases from 0.31 to 0.56. For the two series of targets, the change of specific intensity of reflected wave is very different. When the back thickness is 3 mm, the change of intensity is ruleless. When the back thickness is 6 mm, the intensity improves with the increase of panel thickness.

Comparing the stress waves of the eight kinds of targets, the transmitted waves of the targets with 6 mm-thick back are all stronger than that of the targets with 3 mm-thick back, while the reflected waves of the former are all weaker than the latter. Moreover, the stress waves variation caused by the back thickness is much distinct compared with the slight difference caused by panel thickness. It shows the influence of back thickness on stress wave is much stronger than that of panel thickness. Next the influence of back thickness on the stress waves will be discussed.

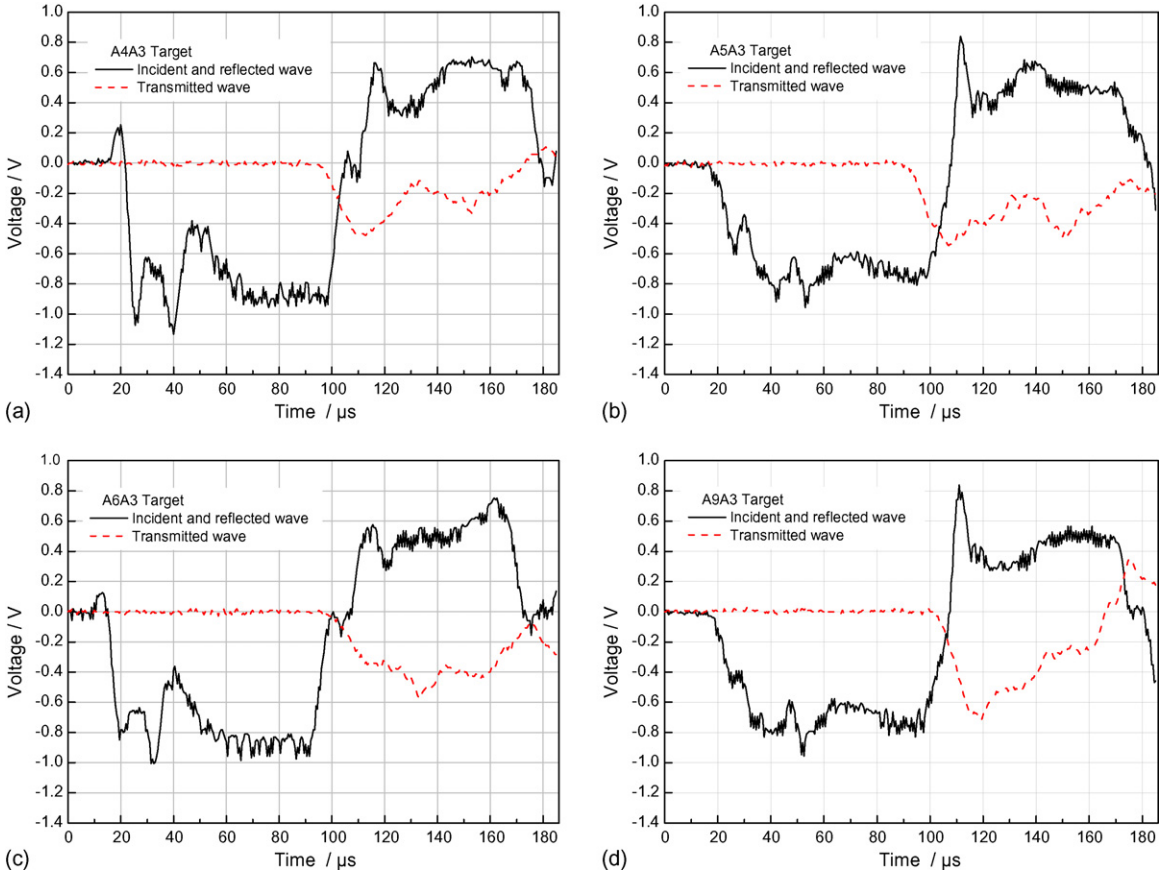

Fig. 9. The stress waves of targets with 3 mm-thick back and different thick panel.

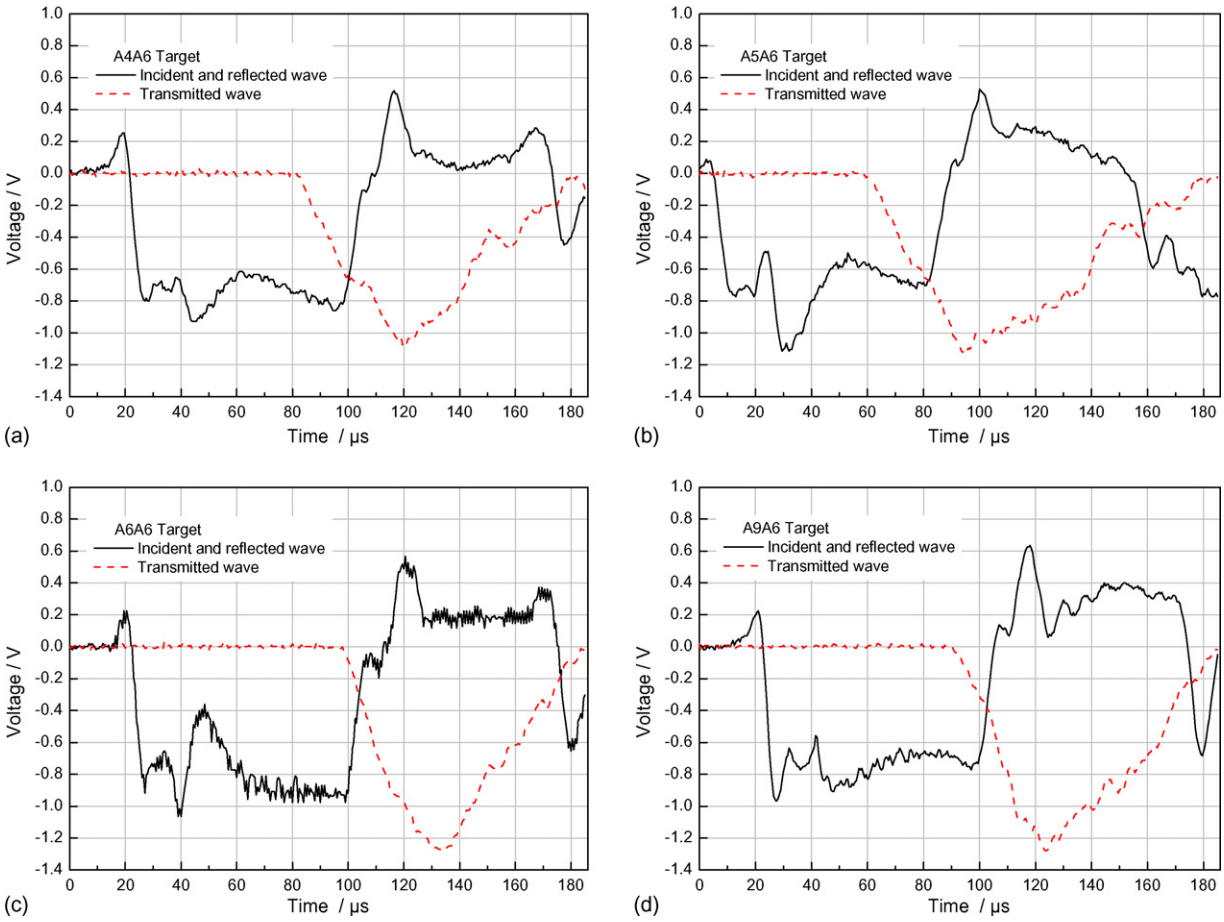

Fig. 10. The stress waves of targets with 6mm-thick back and different thick panel.

3.2.2. Influence of the back thickness

The stress waves of targets with 6 mm-thick panel and different thick back are shown in Fig. 11. The characteristic values of stress waves of the targets are listed in Table 5. With the back thickness increasing from 3 mm to 9 mm, the specific intensity of reflected wave decreases from 0.68 to 0.17. Meanwhile, on the opposite, the specific intensity of transmitted wave increases from 0.44 to 1.23.

When ceramic armors suffered impact load, the ceramic panel is usually destroyed by the reflected stress wave. The increase of back thickness can decrease the reflected stress wave, and therefore it can diminish the damage of ceramic panel effectively. The damages of targets in Fig. 7 also illustrate this point. With the back thickness increase, the damage of ceramic panel reduces significantly. The damage reduction of ceramic panel is beneficial to the impact resistance improvement of armors. By the same token, since the increase of panel thickness can not reduce the reflect stress wave, it can hardly improve the impact resistance of the armors.

On the other hand, the increase of back thickness can reduce the reflected stress wave effectively, but meanwhile, it will enhance the transmitted stress wave. The enhancement of transmitted stress wave will decrease the protection ability of armors. In order to improve the protection ability,

Table 4
Characteristic values of stress waves of the targets with 3 mm-thick back and 6 mm-thick back.

Target	Incident stress wave		Reflected stress wave			Transmitted stress wave		
	Wave length/μs	Intensity/V	Wave length/μs	Intensity/V	Specific intensity	Wave length/μs	Intensity/V	Specific intensity
A4A3	80	−0.777	65	0.536	0.69	74	−0.239	0.31
A5A3	80	−0.684	63	0.515	0.75	75	−0.287	0.42
A6A3	80	−0.758	63	0.516	0.68	70	−0.331	0.44
A9A3	80	−0.679	65	0.460	0.68	70	−0.378	0.56
A4A6	80	−0.731	63	0.156	0.21	85	−0.614	0.84
A5A6	80	−0.703	65	0.216	0.31	90	−0.668	0.95
A6A6	80	−0.781	60	0.240	0.31	75	−0.773	0.99
A9A6	80	−0.732	62	0.311	0.43	78	−0.794	1.08

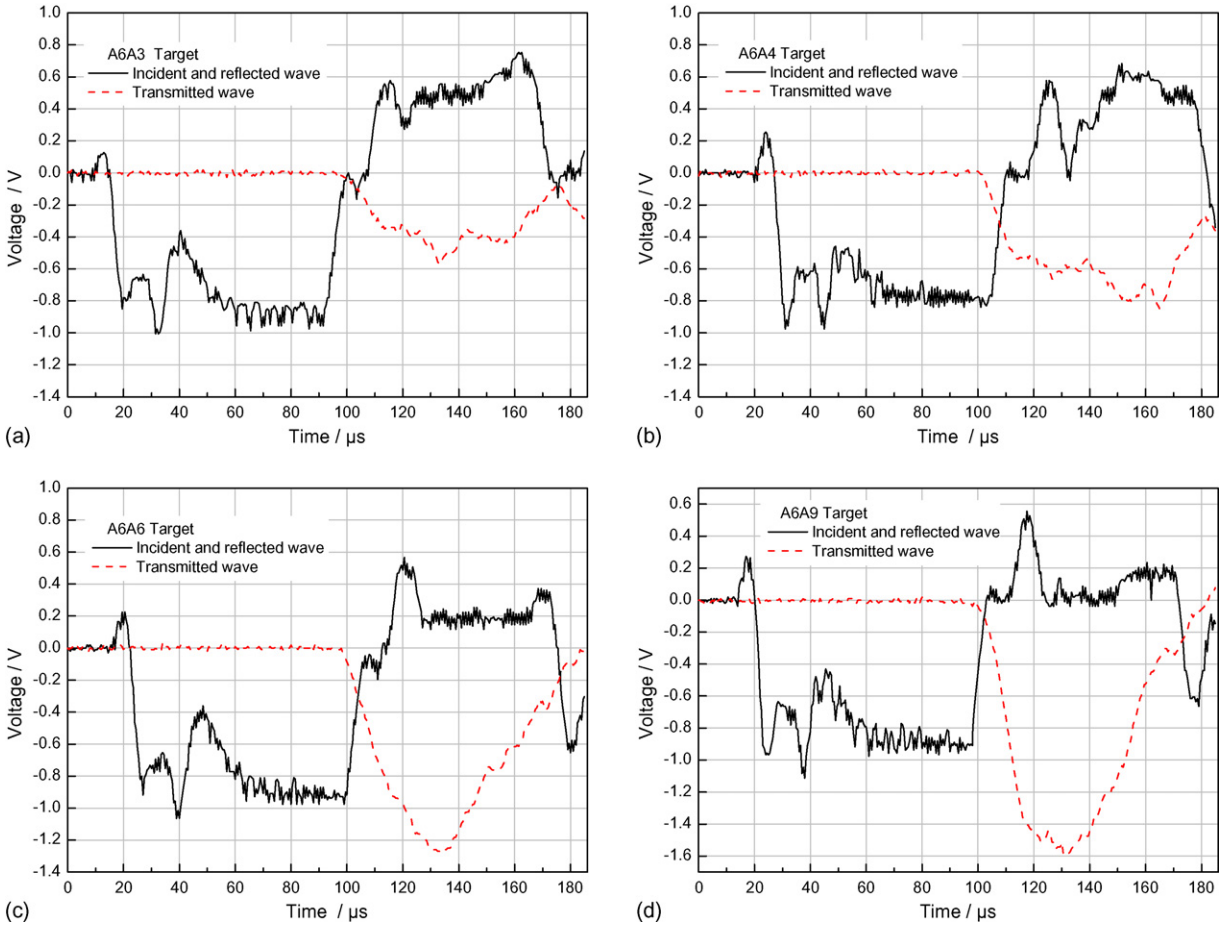

Fig. 11. The stress waves of targets with 6 mm-thick panel and different thick back.

the transmitted stress wave must be absorbed by some other means.

3.3. Failure mechanism analysis of the ceramic panels

Damage of ceramic panels under impact load is mainly a process of formation of radial cracks and cone crack. So, the failure mechanism analysis of the ceramic panel will be focused on the formation mechanism of the two kinds of cracks.

3.3.1. Formation of radial cracks

Radial cracks are tensile cracks, emanating beneath the contact zone in the surface opposite the tile/projectile contact surface. Radial cracks are resulted from the local biaxial bending stresses created by the incident bar in the contact zone.[7] A fracture SEM micrograph of a typical radial crack is shown in Fig. 12. It shows that the radial crack is predominated by a cleavage fracture over its entire area, as could be expected from pure mode I crack in polycrystalline alumina. Because the velocity of the incident bar is only about 15 m/s, the force introduced by it can be regarded as quasi-static. Then, the radial cracks formation problem can be described as a ceramic/metal composite plate resting on a ring support, suffered a quasi-static concentrated load at the center of the plate, the deflection and stress equations can be therefore solved in accordance with thin plate theory.[15]

Table 5
Characteristic values of stress waves of the targets with 6 mm-thick panel.

Target	Incident stress wave		Reflected stress wave			Transmitted stress wave		
	Wave length/μs	Intensity/V	Wave length/μs	Intensity/V	Specific intensity	Wave length/μs	Intensity/V	Specific intensity
A6A0	80	−0.714	70	0.623	0.87	25	−0.174	0.24
A6A3	80	−0.758	63	0.516	0.68	70	−0.331	0.44
A6A4	80	−0.786	62	0.486	0.62	68	−0.588	0.75
A6A6	80	−0.781	60	0.240	0.31	75	−0.773	0.99
A6A9	80	−0.785	58	0.135	0.17	74	−0.966	1.23

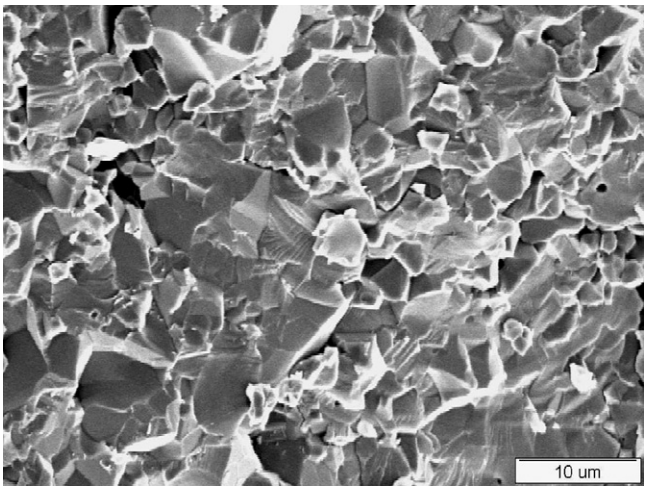

Fig. 12. A fracture SEM micrograph of a typical radial crack.

In accordance with the shell theory, the deflection governing equation of a thin plate can be described as

$$D\left(\frac{\partial^4 w}{\partial x^4} + 2\frac{\partial^4 w}{\partial x^2 y^2} + \frac{\partial^4 w}{\partial y^4}\right) = q(x, y) \tag{4}$$

where D is the bending rigidity of the plate, w is the flexivity function of the plate, and the $q(x, y)$ is the load distribution function. Eq. (4) is a fourth order differential equation, and calculating the deflection of homogeneous plate by it is very complicated. It will be more difficult if using it to solve the deflection problem of a composite plate in present work. In fact, since the composite armor plate suffered a concentrated load, and what concerned is only the deflection and stress beneath the contact zone, the "composite beam" model can be used instead of "composite plate" model. When calculating the deflection and the stress with the "composite beam" model, the problem will be greatly simplified.

A schematic drawing of the composite beam model of composite armor is shown in Fig. 13, assuming the width of the composite is b; the thicknesses of ceramic panel and aluminum are h_c and h_b, respectively. The beam subjected to a concentrated load P in its middle and with the span of $2l$. The distance of neutral face away from the panel/back interface is assumed as h_0, which is positive when neutral face on the alumina side.

The position of neutral face can be calculated as bellow:

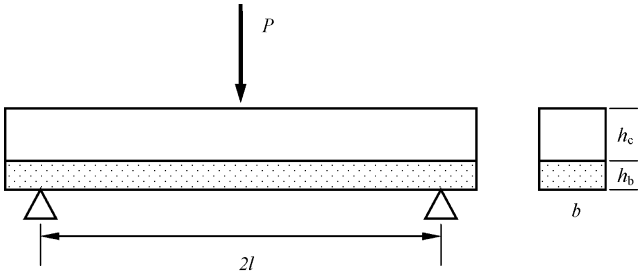

Fig. 13. A schematic drawing of the composite beam model of composite armor.

$$E_c(h_c - h_0)b\left(\frac{h_c - h_0}{2}\right) = E_c h_0 b\left(\frac{h_0}{2}\right) + E_b h_b b\left(h_0 + \frac{h_b}{2}\right),$$

$$h_0 = \frac{E_c h_c^2 - E_b h_b^2}{2(E_c h_c + E_b h_b)} \tag{5}$$

After the neutral face is determined, the inertia moments of the panel and back to the neutral axis can be obtained.

$$I_c = \frac{bh_c^3}{12} + \frac{bh_c(h_c - 2h_0)^2}{4} \tag{6}$$

$$I_b = \frac{bh_b^3}{12} + \frac{bh_b(h_b + 2h_0)^2}{4} \tag{7}$$

The maximum bending moment in the middle of the composite beam is

$$M_{max} = \frac{Pl}{2} \tag{8}$$

Then the curvature radius in the middle of the composite beam can be expressed as

$$\frac{1}{\rho} = \frac{M_{max}}{E_c I_c + E_b I_b} \tag{9}$$

The maximum stress at the panel/back interface of the composite beam is

$$\sigma_{max} = E_c h_0 \frac{1}{\rho} \tag{10}$$

Substituting formula (6)–(9) into formula (10), maximum stress can be expressed as

$$\sigma_{max} = \frac{Pl\, E_c h_0}{2(E_c I_c + E_b I_b)} \tag{11}$$

If making $E_b/E_c = n$, the formula (11) can be changed into

$$\sigma_{max} = \frac{3Pl}{2b[((h_c^3/h_0) + 3h_0h_c - 3h_c^2) + n((h_b^3/h_0) + 3h_0h_b + 3h_b^2)]} \tag{12}$$

where $h_0 = (h_c^2 - nh_b^2)/2(h_c + nh_b)$.

It can be found from formula (12) that the maximum stress in the surface opposite the impact point is controlled mainly by the panel thickness, back thickness, and panel/back moduli ratio when the load is constant. The curves describing the stress variation caused by panel thickness and back thickness with different n can be drawn according to formula (12), as shown in Fig. 14. The stress varying tendencies in Fig. 14 caused by panel thickness and back thickness are distinctly different. When panel thickness is fixed, the stress decreases monotonously with the increase of back thickness. On the other hand, when back thickness is fixed, the stress increases firstly and then decreases after reaching a maximum value with the increase of panel thickness.

The stress variation with different panel/back moduli ratio can also be found in Fig. 14. Firstly, when the panel and back thickness is fixed, the stress increases with the increase of panel/back moduli ratio. Secondly, with the increase of n, the stress declines more sharply when back thickness increases, and the peak of the stress variation curve is more evenly when panel thickness is different. For example, when n is 0.5, the curve has

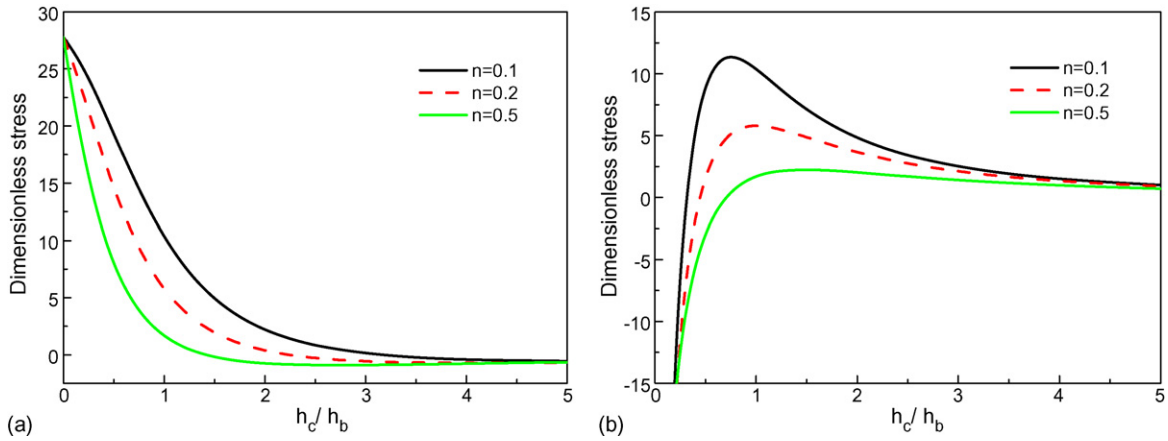

Fig. 14. The stress variation caused by panel thickness and back thickness with different panel/back moduli ration, (a) back thickness changes with panel thickness fixed; (b) panel thickness changes with back thickness fixed.

almost no peak and the stress is almost same on the right side of the peak with panel thickness increase.

Since the formation of radial cracks is predominated by the maximum bending stress in the surface opposite the impact point, the stress can be used to estimate the number of radial cracks. The larger the stress, the more radial cracks will form. The dimensionless stresses of some targets discussed above were calculated by formula (12) and listed in Table 6. The variation tendencies of the stress and the number of radial cracks are accordant when the back thickness changes on the left of the table. On the opposite, the variation tendencies of the parameters are reversed when the back thickness changes on the right. It shows there are still errors in the "composite beam" model. Even so, when considering the targets as a whole, the targets with higher calculated stress can be found more radial cracks. So the formula (12) can still be used to estimate the number of radial cracks by the large for ceramic composite armor design.

3.3.2. *Formation of cone crack*

There are two kinds of viewpoints generally about the cone crack formation mechanism in ceramic panels. The formation of cone crack was considered to be controlled by semi-static failure mechanism in most studies when impact velocity smaller than 700 m/s.[3,7,16] Another kind of viewpoints considering the stress wave effect, argued that the cone crack formation is controlled by the tensile stress waves reflected from the panel/back interface and the edge face of the ceramic panel.[17–19] Sherman[7] investigated the damages of confined alumina/steel armors under bullet impact, suggesting that the formation was controlled by semi-static mechanism. He considered that the cone crack formed near the projectile/panel contact zone and expanded to the bottom of the panel. In order to find out the formation mechanism of the cone crack, the fracture morphologies of the ceramic inverted cone shown in Fig. 15 were inspected carefully.

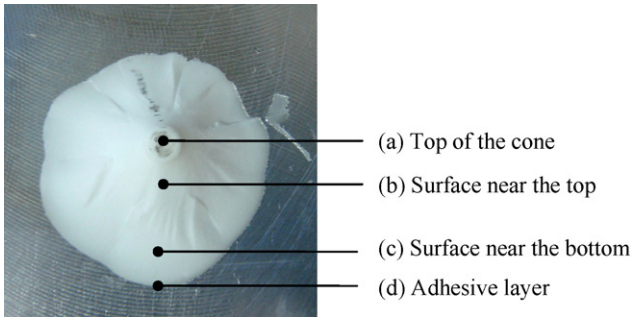

Fig. 15. The intact ceramic inverted cone of A6A9 for fracture micrograph analysis.

Fig. 16 shows the micrographs of the top of the ceramic cone. A platform in the center of the top can be observed from Fig. 16(a). There is a discontinuity zone existed between the platform and the cone crack surface. The micrograph in Fig. 16(b) shows a typical appearance of compressive damage, in which the crystal grains on the top were crushed and edges of them were ground blunt. At the same time, there is no expanded crack observed from Fig. 16, indicating that no compression damage crack formation in the impact zone.

Fig. 17(a) and (b) is the micrographs of the cone crack surface near the cone top and near the cone bottom, respectively. It was found the fracture mode over the entire cone crack surface is cleavage fracture. Shear fracture characteristic described in literature[6,7] was not found in the cone crack surface. So the cone crack formation was suggested dominated by tensile tress.

Table 6
The comparison of maximum bending stress in the panel and the number of radial cracks.

Target	Dimensional stress calculated	Number of radial cracks	Target	Dimensional stress calculated	Number of radial cracks
A6A3	14.9	9	A4A3	21.6	8
A6A4	11.2	8–9	A5A3	18.1	9
A6A6	6.0	4–7	A6A3	14.9	9
A6A9	2.1	2	A9A3	8.5	11

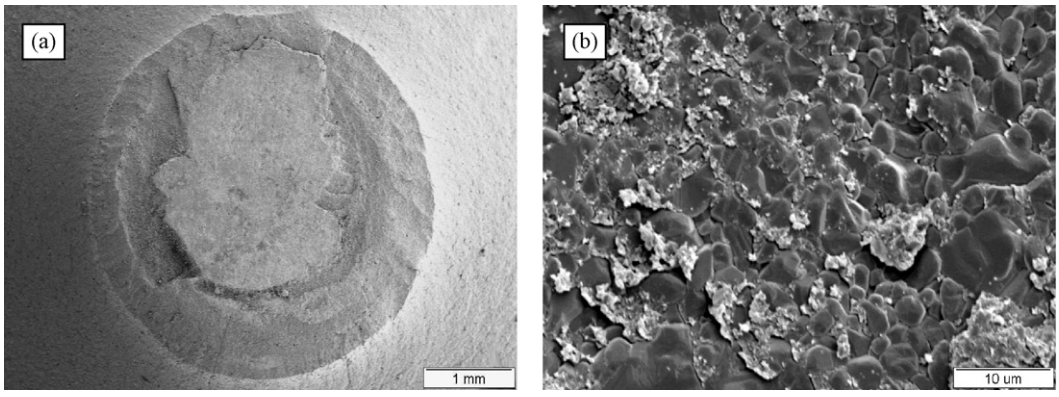

Fig. 16. The SEM micrographs analysis for fracture surface of the cone crack, (a) a vertical view, 50×; (b) the micrograph in the center of the top surface of the cone, 5000×.

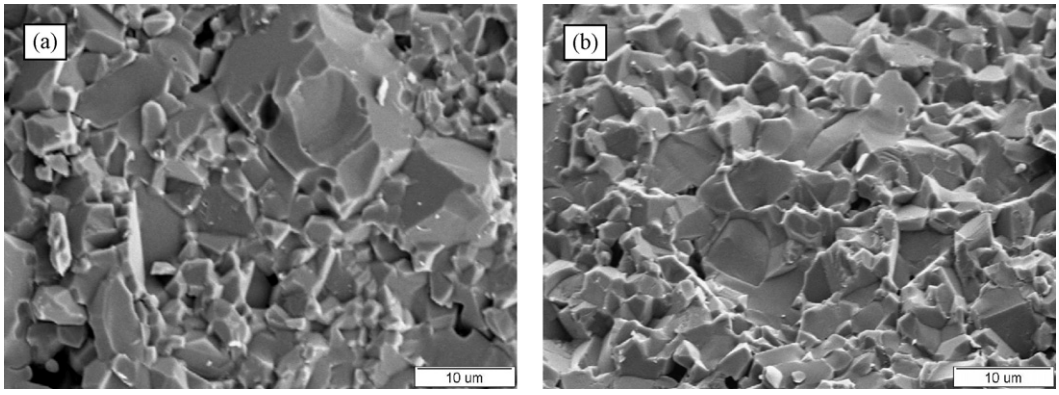

Fig. 17. The SEM micrographs analysis for the top of the ceramic cone, (a) the surface near the top, 5000×; (b) the surface near the top, 5000×.

However, the propagation direction of the cone crack cannot be judged from the fracture morphology.

Fig. 18 gives the fracture morphology of adhesive layer between the alumina panel and aluminum back. Images in Fig. 18 displayed typical brittle fracture morphology, the crack propagation direction can be judged by the river patterns formed through the fracture surface. The river patterns in Fig. 18(a) and (b) both displayed that the crack propagating from the adhesive/back interface to panel/adhesive interface, it means that the cone crack formed at the bonding face of the ceramic panel and expanded to the impact face. So the cone crack formation should be dominated by the stress wave mechanism instead of semi-static mechanism.

Some particular characteristics of macro-appearance of the ceramic cone cavities can confirm the stress wave control mechanism of cone crack formation. As shown in Fig. 19(a), multi-layer cone cracks can be observed in the alumina panel after gold spray treatment. The multi-layer cracks shaped when the stress wave reflected again from the crack surface formed by the first reflected stress wave. It is a typical characteristic of stress wave damage. The multi-layer cone cracks appearance cannot be explained by the semi-static mechanism. Fig. 19(b)

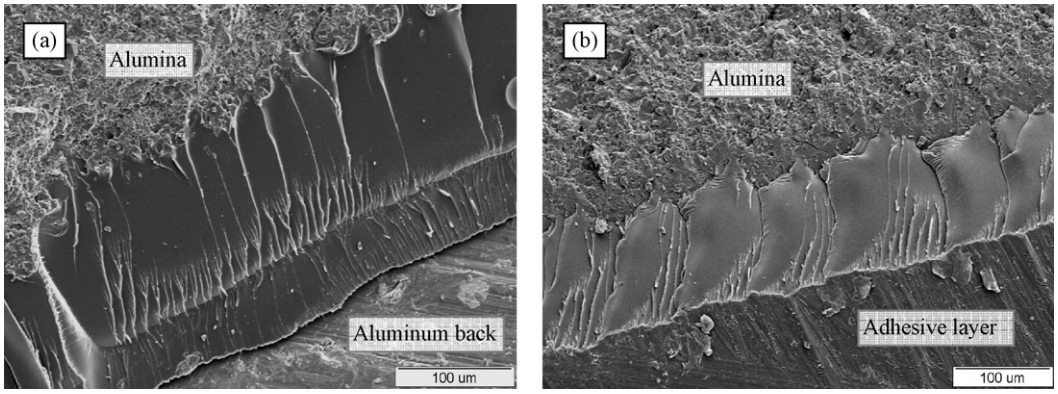

Fig. 18. The SEM micrographs analysis for the fracture surface of the adhesive layer between the panel and back, (a) the view of the adhesive layer beneath the ceramic inverted cone, 600×; (b) the adhesive layer on the edge of the ceramic inverted cone cavity, 500×.

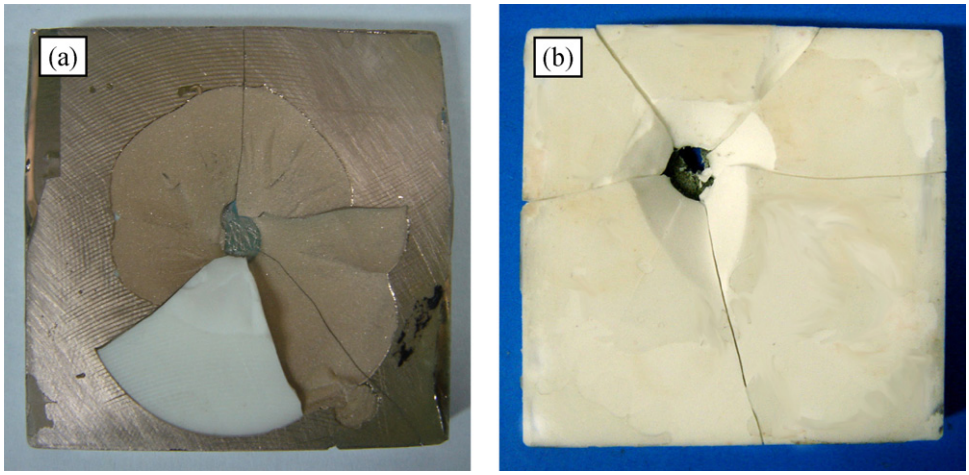

Fig. 19. The appearance of the ceramic inverted cone cavities, (a) the multi-layer cone cracks; (b) the unsymmetrical cavity formed with impact aside from the center.

shows an unsymmetrical ceramic inverted cone cavity formed by the impact aside from the center of the target. The decline angle variation of different section of cone crack can be explained by the distance variation of the stress wave traveled from the impact point to the side surface of the ceramic panel. For the sections near panel side, the stress wave travel distance is short, so the cone vertex angle is smaller. For the sections far from panel side, the stress wave travels a longer distance, and then the cone vertex angle is larger.

The analysis above confirmed that the cone crack formation in ceramic panels is controlled by the stress wave mechanism. Despite the impact velocity of incident bar is quite low, the tensile stress wave formed in the ceramic panel is sufficient to destroy the ceramic panel and cause the cone crack. In this sense, the stress wave caused by the bullet impact will stronger much than that caused by incident bar, so the cone crack formation will be no doubt controlled by stress wave mechanism.

Of cause, some effects in ballistic impact such as local deformation of back and comminution of ceramic cannot be simulated by low velocity SHPB. The results in low velocity impact may not be transferred directly to ballistic impact. Even though, the SHPB can provide enough impact causing radial cracks and cone crack, which have to be proved as the main failure mechanisms of ceramic panel. In addition, the SHPB can present damage character transformation of ceramic panel as armor structures change. In this regard, the modified SHPB is appropriate for damage mechanism study of ceramic armor and worth to make more efforts.

4. Conclusions

In order to simulate the behavior of projectile impacting on target better, the incident bar and the transmitted bar of the SHPB device were modified. Using the modified SHPB device, the impact tests of alumina/aluminum composite armors with different panel/back thickness ratio were carried out. The damage characteristics and stress wave features of the targets under impact were investigated, especially the influence of panel thickness and back thickness on them were studied in detail. Furthermore, the failure mechanism of the ceramic panels, including the radial cracks and the cone crack formation mechanism was analyzed. Through the study, several beneficial conclusions can be got as bellow.

The influences of panel thickness and back thickness on the stress wave features are different. With the increase of back thickness, the intensity of transmitted stress wave increased and the intensity of reflected stress wave decreased, and the damage of ceramic panels reduced significantly. It is beneficial to the ballistic performance of composite armors. Compared with the back thickness, the change of the panel thickness of armors has insignificant influence on the stress wave propagation features.

The impact damage morphology analysis of the composite armors showed that the vertex angle of ceramic inverted cone increased with the back thickness increase and panel thickness decrease. The number of radial cracks in ceramic panels reduced with the increase of back thickness and decrease of panel thickness.

Damage mechanism analysis of ceramic panel showed that the radial cracks formation is controlled by semi-static failure mechanism. The number of radial cracks is related to the local biaxial bending stress on panel bonding face caused by deflection under impact load. The number of radial cracks increases with the increase of local bending stress. The “composite beam” model was established to estimate the local bending stress. The model calculation showed that the local bending stress is related to the panel thickness, back thickness and the panel/back moduli ratio. When panel thickness is fixed, the stress decreases monotonously with the increase of back thickness. When back thickness is fixed, the stress increases firstly and then decreases after reaching a maximum value with the increase of panel thickness. When the panel and back thickness are both fixed, the stress increases with the increase of panel/back moduli ratio. The model can be used to predict the number of radial cracks in ceramic panels. The fracture characteristic and macro-morphology analysis of cone crack argued that the cone crack formation is dominated by the stress wave damage mechanism.

References

1. Goncalves, D. P., de Melo, F. C. L., Klein, A. N. and Al-Qureshi, H. A., Analysis and investigation of ballistic impact on ceramic/metal composite armour. *International Journal of Machine Tools & Manufacture*, 2004, **44**, 307–316.
2. Timothy, J. H. and Gordon, R. J., Modeling prestressed ceramic and its effect on ballistic performance. *International Journal of Impact Engineering*, 2005, **31**, 113–127.
3. Fawaz, Z., Zheng, W. and Behdinan, K., Numerical simulation of normal and oblique ballistic impact on ceramic composite armours. *Composite Structures*, 2004, **63**, 387–395.
4. López-Puente, J., Arias, A., Zaera, R. and Navarro, C., The effect of the thickness of the adhesive layer on the ballistic limit of ceramic/metal armours. An experimental and numerical study. *International Journal of Impact Engineering*, 2005, **32**, 321–336.
5. Chocron Benloulo, I. S. and Sánchez-Gálvez, V., A nes analytical model to simulate impact onto ceramic/composite armors. *International Journal of Impact Engineering*, 1998, **21**, 461–471.
6. Sherman, D., Impact failure mechanisms in alumina tiles on finite thickness support and the effect of confinement. *International Journal of Impact Engineering*, 2000, **24**, 313–328.
7. Sherman, D. and Ben-Shushan, T., Quasi-static impact damage in confined ceramic tiles. *International Journal of Impact Engineering*, 1998, **21**, 245–265.
8. Franzen, R. R., Orphal, D. L. and Anderson Jr, C. E., The influence of experimental design on depth-of-penetration (DOP) test results and derived ballistic efficiencies. *International Journal of Impact Engineering*, 1997, **19**, 727–737.
9. Ben-Dor, G., Dubinsky, A. and Elperin, T., Optimization of two-component composite armor against ballistic impact. *Composite Structures*, 2005, **69**, 89–94.
10. Zhao, Han and Gary, Gérard, On the use of SHPB techniques to determine the dynamic behavior of materials in the range of small strains. *International Journal of Solid Structures*, 1996, **33**, 3363–3375.
11. Tasdemirci, A. and Hall, I. W., The effects of plastic deformation on stress wave propagation in multi-layer materials. *International Journal of Impact Engineering*, 2007, **34**, 1797–1813.
12. Zhao, H., Elnasri, I. and Abdennadher, S., An experimental study on the behaviour under impact loading of metallic cellular materials. *International Journal of Mechanical Sciences*, 2005, **47**, 757–774.
13. Song, Bo, Chen, W. W. and Dou, S., Strain-rate effects on elastic and early cell-collapse responses of a polystyrene foam. *International Journal of Impact Engineering*, 2005, **31**, 509–521.
14. Hetherington, J. G. and Rajafopalan, B. P., An investigation into the energy absorbed during ballistic perforation of composite armors [J]. *International Journal of Impact Engineering*, 1991, **11**(1), 33–40.
15. Berthelot, J.-M., *Composite Materials Mechanical Behavior and Structural Analysis*. Springer, 1998, pp. 304–310. Translated by J. Michael Cole.
16. Denoual, C., François Hild dynamic fragmentation of brittle solids: a multi-scale model. *European Journal of Mechanics: A Solids*, 2002, **21**, 105–120.
17. Bruck, H. A., A one-dimensional model for designing functionally graded materials to manage stress waves. *International Journal of Solids and Structures*, 2000, **37**, 6383–6395.
18. Mariotti, C., Perlat, J. P. and Guérin, J. M., A numerical approach for partially saturatedgeomaterials under shock. *International Journal of Impact Engineering*, 2003, **28**, 717–741.
19. Mines, R. A. W., A one-dimensional stress wave analysis of a light weight composite armour. *Composite Structures*, 2004, **64**, 55–62.